Article

Journal of the Brazilian Chemical Society

https://dx.doi.org/10.21577/0103-5053.20230173

J. Braz. Chem. Soc. **2024**, *35*, 5, e-20230173, 1-17

In silico Analysis of Natural Products from Brazilian Biodiversity in COVID-19 Treatment: NuBBE Database against SARS-CoV-2 Papain-Like Protease

Caio Felipe A. R. Cheohen, [*,#,a] *Maria Eduarda A. Esteves,* [#,b,c] *Vinnícius M. S. Gomes,* [a] *Diego Allonso* [d] *and Manuela L. da Silva* [*,a,b,c]

[a]*Laboratório Integrado de Biologia Computacional e Pesquisa em Ciências Farmacêuticas (LAMCIFAR), Instituto de Biodiversidade e Sustentabilidade NUPEM, Centro de Ciências da Saúde, Universidade Federal do Rio de Janeiro, 27965-045 Macaé-RJ, Brazil*

[b]*Laboratório de Macromoléculas (LAMAC), Instituto Nacional de Metrologia, Qualidade e Tecnologia, Av. Nossa Sra. das Graças, 50, Xerém, 25250-020 Duque de Caxias-RJ, Brazil*

[c]*Programa de Pós-Graduação em Biologia Computacional e Sistemas, Instituto Oswaldo Cruz/Fiocruz, Av. Brasil, 4365, Manguinhos, 21040-900 Rio de Janeiro-RJ, Brazil*

[d]*Departamento de Biotecnologia Farmacêutica, Faculdade de Farmácia, Centro de Ciências da Saúde, Universidade Federal do Rio de Janeiro, Ilha do Fundão, 21941-902 Rio de Janeiro-RJ, Brazil*

Coronavirus disease (COVID-19) pandemic has infected 630 million people and led to 6.59 million deaths worldwide since its outbreak. To control COVID-19 advance, finding new molecules with potential to inhibit viral spread is pivotal. Papain-like protease (PLpro) is one of the most interesting targets of pharmacological inhibition since it is implicated not only in viral replication but also in modulation of host immune response. Natural products are of great interest to the pharmaceutical industry due to their diverse structure and biological activities. The NuBBEDB (Nuclei of Bioassays, Biosynthesis and Ecophysiology of Natural Products Database) is an excellent source of natural products (NPs) from the Brazilian flora. In this study, we performed virtual screening, molecular dynamics, and binding energy analyses of the NuBBEDB library to target severe acute respiratory syndrome coronavirus 2 (SARS-CoV-2) papain-like protease (PLpro), the virus's protease essential for replication. Among the top-ranked molecules, the indole alkaloids raputindoles A, C, and D emerged as potential SARS-CoV-2 inhibitors, showing significant interactions with the pivotal Beta-Loop-2 (BL2) region, including the catalytic Y268 residue. Notably, raputindole D displayed enhanced stabilization of the BL2 region, while raputindole C exhibited superior overall stability. These *in silico* findings suggest that raputindoles, especially D, might offer therapeutic value against COVID-19, laying the groundwork for further experimental evaluations.

Keywords: coronavirus, *in silico* analysis, *Raputia praetermissa*

Introduction

In March 2020, the World Health Organization declared the coronavirus disease (COVID-19) pandemic.[1] Since then, the severe acute respiratory syndrome coronavirus 2 (SARS-CoV-2), the etiologic agent of COVID-19, has infected over 766 million individuals worldwide, from which approximately 6.9 million deaths occurred.[2] Among COVID-19 survivors, symptoms such as fatigue, dyspnea, headaches, and palpitations become usual, what is now classified as post-covid syndrome.[3] Therefore, identifying molecules that inhibit viral infection and its deleterious effects on human health is crucial. Vaccination has played a crucial role in controlling COVID-19 advance; however, the quick decrease of neutralizing antibodies induced by vaccine along the time with the emergence of new virus variants[4] make alternative strategies to inhibit viral replication urgent and relevant. Vaccines and drugs have different objectives, while vaccines stimulate the production of antibodies and prevent infection, drugs treat patients who are already infected.[5] In this context, inhibition of key viral enzymes, such as virus proteases, plays a significant role in the context of antiviral inhibitors.[6]

*e-mail: caiocheohen@ufrj.br; manuleal@gmail.com
#Both authors contributed equally to this work.
Editor handled this article: Paula Homem-de-Mello (Associate)

Papain-like protease (PLpro) is a SARS-CoV-2 protease that cleaves interferon-stimulated gene 15 (ISG15), hijacking its amino terminal ubiquitin-like domain, thus compromising type I interferon (IFN) response,[7,8] which drives immune cells into pro-inflammatory profile.[9] In addition, PLpro plays another role in SARS-CoV-2 infection. During the course of infection, a single-stranded positive-sense viral ribonucleic acid (RNA) is processed, which generates two polypeptides: pp1a and pp1b.[9,10] PLpro cleaves the polyproteins at nsp1, nsp2 and nsp3 sites, generating individual and functional enzymes, therefore, its activity is pivotal for proper viral transcription and replication processes.[9,11] Thus, PLpro inhibition hampers not only viral replication but also virus-induced host immune modulation, making it a potential pharmacological target to be explored.[7,12] Several studies have already targeted PLpro for drug development,[13-15] using natural products (NPs)-bioactive compounds derived from plants, animals, and microorganisms-as a potential and relevant source of new inhibitor compounds.[11,16]

NPs are of great interest to the pharmaceutical industry due to their numerous and diverse biological structures and activities. Among them, plants are one of the most remarkable sources of these products.[17] Brazil is a hotspot for natural products (NPs) due to its huge biodiversity.[18] Several NPs are included in the NuBBEDB (Nuclei of Bioassays, Biosynthesis and Ecophysiology of Natural Products Database), a database created in 2013 that has grown and improved since then.[18,19] It contains not only NPs but also their sources, such as species phylogenetic information, correlation heatmaps between sources/metabolic classes and their therapeutic effects, among some other features.[19]

Therefore, in this study, we searched at NuBBEBD potential PLpro inhibitors using *in silico* approaches. We found twenty-one potential molecules, including three raputindoles, which is a group of indoles isolated from a dichloromethane extract of *Raputia praetermissa* that proved to be the most promising molecules analyzed in this study.[20]

Methodology

Construction of receptors and ligands models

The *in silico* interactions between PLpro against the NuBBEDB were evaluated through docking simulations using the AutoDock (Vina),[21] and GOLD Suite software (score function: ChemPLP and GoldScore),[22] while the final consensus score was calculated through the results of Vina, ChemPLP, and GoldScore.

Redocking parameters were established for screening substances using the three scoring functions. To carry out step (Vina), the pK_a of the PLpro (PDBid 7JRN) was performed using the PROPKA 3.0 software[23] through PDB2PQR[24] with AMBER force field, and pK_a of ionizable protein residues at pH 7.4. The probable protonation states of this GRL0617 ligand that is complexed to 7JRN were adjusted. The conversion of the PLpro structure into the pdbqt file format was performed using the PDB2PQR output in UCSF Chimera.[25]

Molecular docking and virtual screening

The redocking of PLpro was simulated in exhaustiveness 100 in (Vina) and the root mean square deviation (RMSD) was calculated with OpenBabel between the first pose from the docking of each exhaustiveness and the original ligand, GRL0617 (PDBid 7JRN), which was extracted from the A chain of the three-dimensional structure of PLpro.

Redocking was also performed for steps ChemPLP and GoldScore). Binding site parameters were set to a radius of 10 Å from the center of GRL0617 and had its water molecules removed for redocking. The protonation states of the residues were adjusted to pH 7.4 according to the pK_a prediction calculated by the PDB2PQR.

Following these parameters, the simulation was performed using ChemPLP and GoldScore. The GOLD software performed a re-score through "ASP" score function, whereupon the RMSD value was calculated, and the selection of the best ligand pose was generated for each simulation. GOLD function values were exhibited as the name "score" for the GOLD/CHEMPLP, and "fitness" for the GOLD/GoldScore.

The interactions of amino acid residues N267, Y268 and Q269, with ligand GRL0617, were evaluated using Discovery Studio Visualizer (DSV)[26] and compared to the redocking results performed on the AutoDock (Vina) and GOLD complexed to the receptor protein.[21,22,27]

Classification model

The virtual screening results were classified following a penalty score. The penalty score was performed as the higher classification of the molecule in the molecular docking results, the lower the penalty suffered. The penalty score had a range between zero and one, where values closer to zero indicate a better molecule in the final consensus score.

Filtering by pharmacokinetic parameters

Pharmacokinetic parameters were predicted by using the SwissADME[28] and the pkCSM[29] servers, and DataWarrior

software,[30] and ADMETlab 2.0.[31] Thus, through the prediction of programs, we applied filters related to molecular size: molecular weight (MW) ≤ 1000 Da, absorption: hydrogen bond donors (HBD) ≤ 6, hydrogen bond acceptors (HBA) ≤ 15 and number of rotatable bonds (NRotB) ≤ 20. Other parameters were analyzed in a complementary way. Acceptable values for lipophilicity are −2 ≤ cLogP (calculated Log partition coefficient) ≤ 10, absorption: Caco2 > 0.90 (pkCSM) or ≤ −5.15 log cm s^{-1} (ADMETlab 2.0), intestinal absorption > 30% (pkCSM) or < 0.3 (ADMETlab 2.0). In addition to the ability to be a P-glycoprotein (Pgp) inhibitor or substrate, for ADMETlab 2.0 < 0.3. Likewise, blood-brain barrier (BBB) permeability, the probability of being a cytochrome P450 (CYP) inhibitor or substrate, and the ability to cause respiratory toxicity are represented as high for values < 0.3. In addition, we evaluated the toxicological parameters: hepatotoxicity, mutagenicity and tumorigenicity.

Interaction analysis

Interaction analysis of the NPs previously classified as promising was re-evaluated. The best-ranked molecules from steps (Vina), (ChemPLP) and (GoldScore) were analyzed using DSV based on the receptor-ligand complex interaction and residues of interest (Y268, N267 and Q269).

Molecular dynamics and molecular mechanics/Poisson-Boltzmann surface area (MM/PBSA) analysis

We conducted three replicates of molecular dynamics simulations using the GROMACS 2020.4 package for protein-ligand complexes comprising the PLpro receptor and raputindoles A, C, and D. These complexes were generated through virtual screening using Autodock Vina. Additionally, to enable comparison with the values obtained for the hits, we performed the same set of simulations for GRL0617.[32,33] The CHARMM36 (C36) force field (FF) was employed for these simulations.[34,35]

The ligands were prepared using the CHARMM General Force Field (CGenFF) program, accessed through the CGenFF.[36,37]

To configure the system, the "gmx editconf" utility was utilized. The system was then positioned within a dodecahedron box, ensuring a 1.0 nm distance from the box's edge to any atom within the system. Subsequent solvation was done using the TIP3P water model. System neutralization was achieved by adding two chloride (Cl) ions.

Energy minimization employed the steepest descent method, which was halted when the maximum force dropped below 1000.0 KJ mol^{-1}. The energy step was designated as 0.01, with a cap placed at 50,000 minimization steps. A grid-based neighbor search was used, set with a list size of 1 and a 1.2 nm cutoff distance. Electrostatic interactions were managed using the Particle Mesh Ewald (PME)[38] method with a 1.2 nm cutoff. Van der Waals interactions were similarly processed with a 1.2 nm cutoff. The system was treated as fully periodic, and no long-range dispersion corrections were applied to energy or pressure calculations.

The production molecular dynamics (MD) simulation ran for a total of 50 ns and was executed in graphics processing unit (GPU) mode. Electrostatics over long-ranges were managed using PME, with a configuration of 1 PME rank coupled with 5 OpenMP threads. The gmx hbond tool in GROMACS[32,33] was used to calculate the number of hydrogen bonds between the protein-ligand complexes during the whole simulation. Furthermore, the gmx_MMPBSA[39,40] script was employed to estimate binding free energy (ΔG) analysis. MM/PBSA was performed at every 50 ps from the molecular dynamics.[41] RMSD, root mean square fluctuation (RMSF), and hydrogen bond analyses were visualized using Matplotlib.[42]

Results

It was set a panel of 2,162 NPs from NuBBEDB and it was analyzed their potential to inhibit the PLpro activity, as determined by *in silico* analysis. NPs underwent virtual screening in Vina, ChemPLP and GoldScore. The compounds best ranked for the consensus (penalty) score had their absorption, distribution, metabolism, excretion, and toxicity (ADMET) characteristics predicted. Analyses of interactions of PLpro residues with ligands were performed in order to elucidate the interaction profile of these NPs.

Molecular docking and virtual screening

N267, Q269 and the main residue Y268 have been previously described in the Beta-Loop-2 (BL2) region of the PLpro enzyme. Interactions with these residues indicate that the testing compound would probably inhibit the enzyme catalytic activity and, therefore, has the potential to inhibit SARS-CoV-2 replication.[43]

The PLpro inhibitor GRL0617 is found in PDB 7JRN and has been used before to validate the selected method through molecular redocking.[44] The first binding mode generated in the redocking (Figure 1) with Vina presented a binding energy of −9.6 kcal mol^{-1} and RMSD of 0.45 Å. When redocking was performed using ChemPLP, the score was 90.41 with an RMSD of 0.54 Å. In comparison, the

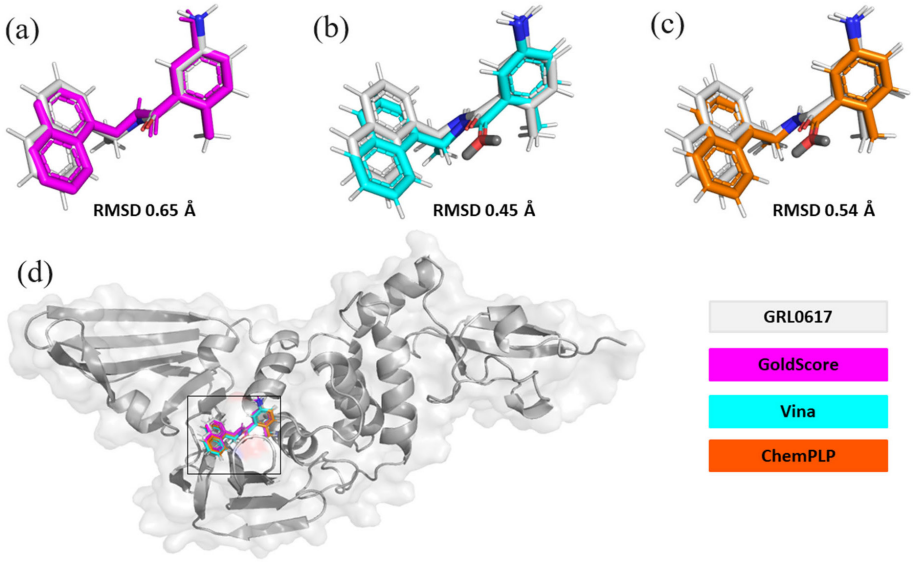

Figure 1. Redocking results: complex PLpro and ligand GRL0617 (PDB id: 7JRN) (in grey). (a) Gold score (magenta); (b) AutodockVina (ciano); (c) ChemPLP (orange); (d) redocking ligands overlap the PLpro binding site.

simulation with GoldScore yielded a score of 59.35 and an RMSD of 0.65 Å, when evaluated against GRL0617.

After virtual screening, it was selected 21 molecules that accomplished a penalty score value lower or equal to 0.05 to interaction analysis. These molecules belonged to six different chemical classes, namely flavonoids (8), alkaloids (4), aromatic derivatives (4), chalcones (4), polyketides (3) and phenylpropanoids (1) (Table 1).

Among these chemical classes, flavonoids and alkaloids stood out for their already known capacity of viral inhibition.[11,45,46]

In addition, our previous study[11] showed that flavonoids from *Siparuna cristata* have properly inhibited PLpro based on virtual screening and *in vitro* analysis. Based on this, the identification of 8 flavonoids in the current study indicates that the applied methodology can mimic the real interactions occurring between the compounds and the PLpro enzyme.

Interestingly, we found that from four alkaloid molecules, three are raputindoles, with raputindoles C, A, and D ranking 11th, 15th, and 16th places, respectively. The other alkaloid on this list, named 1,3,5-trihydroxy-4-methoxy-10-methyl-2,8-bis(3-methylbut-2-nyl)acridin-9(10*H*)-one, ranked the 21st position.

Analysis of the interactions between rapuntidoles and the PLpro enzyme

Raputindole C

Raputindole C interacted with the main residue Y268 in all analysis performed (ChemPLP, GoldScore, and Vina, Figures 2b, 2d and 2f, respectively). We observed that the interactions occurred between the aromatic rings of the pi-pi T-shaped type, and the amide-pi stacked occurring at 4.85 Å (Vina, Figure 2e) and 4.65 Å (GoldScore, Figure 2c), while for ChemPLP, two interactions of the pi-pi T-shaped type 4.82 and 4.78 Å (Figure 2a) were simulated. A difference of only 0.20 Å between the longest and shortest distance were found among the three different methodologies applied in this study, which indicates a consensus, not only for the penalty scores but also for the interaction analyses. Alkyl and pi-alkyl interactions were also found to occur at 4.33 Å (GoldScore, Figure 2c), 4.82 Å (Vina, Figure 2e) and 5.43 Å (ChemPLP, Figure 2a). It was found pi-sigma interactions between the ligand and the Q269 residue in all simulations, at 3.88 Å (Vina, Figure 2e), 3.97 Å (ChemPLP, Figure 2a) and 3.86 Å (GoldScore, Figure 2c). Finally, it was also observed the occurrence of van der Waals interactions with residue N267 in (Vina) and (ChemPLP).

Raputindole A

It was observed distances between 4.99 and 5.88 Å for the interactions between PLpro Y268 residue and raputindole A (Figures 3b, 3d and 3f). Pi-pi T-shaped and amide-pi stacked interactions occurred at 5.26 and 5.48 Å in Vina (Figure 3e), 5.17 and 5.30 Å in ChemPLP (Figure 3b), and 5.03 and 5.50 Å in (GoldScore, Figure 3d). Alkyl and pi-alkyl interactions occurred between 4.99 and 5.79 Å (Vina, Figure 3f), a single interaction at 5.88 Å was seen in ChemPLP (Figure 3b), and at 5.97 Å in (GoldScore, Figure 3d). Only carbon-hydrogen interactions were found for Ans267, occurring between 4.49 Å (Vina, Figure 3f), 3.92 Å (ChemPLP, Figure 3b) and 3.89 Å (GoldScore, Figure 3d). Simulated interactions with Q269 showed alkyl and pi-alkyl at 4.49 Å (ChemPLP), and pi-pi T-shaped while amide-pi stacked were observed at

Table 1. NuBBEDB ID name and class of 21 molecules best ranking according to the penalty score (≤ 0.05), by order of classification

Classification	NuBBEDB ID	Molecule name	Class
1	200	amentoflavone	flavonoids
2	272	1,6-di-*O*-caffeyoyl-β-D-glucopyranoside	phenylpropanoids
3	198	amentoflavone 7'',4''-dimethyl ether	flavonoids
4	558	kaempferol-3-*O*-α-L(4''-*Z*-*p*-coumaroyl)-rhamnoside	flavonoids
5	199	podocarpusflavone A	flavonoids
6	2002	(2*R*)-7,4'-dibenzyl-5-hydroxy-3'-methoxy-6,8-dimethylflavanone	flavonoids
7	875	1-[3-(3,7-dimethylocta-2,6-dien-1-yl)-2,4,6- trihydroxyphenyl]-3-(4-hydroxyphenyl)propan-1-one	chalcones
8	1639	2,6-nonadienoic acid, 9-[6-(acetyloxy)-3,4-dihydro-2,8-dimethyl-2*H*-1-benzopyran-2-yl]-6-methyl-2-(4-methyl-3-pentenyl)-,(*Z*,*E*)-	aromatic derivatives
9	119	pterogynoside; kaempferol-3-*O*-(3''-*O*-4'''-methylgallate-α-L-rhamnoside)	flavonoids
10	197	heveaflavone	flavonoids
11	1136	raputindole C	alkaloids
12	2329	1-propanone, 3-[3-hydroxy-4-methoxy-5-(3-methyl-2-buten-1-yl)phenyl]-1-[2,4,6-trihydroxy-3-(3-methyl-2-buten-1-yl)phenyl]-	chalcones
13	521	(*S*)-MPA-5'-epichaetoviridin A	polyketides
14	279	7-methyl-sargachromenol; 2,7,8-trimethyl-2-[(3-*E*,7-*Z*)-4,12-dimethyl-8-carboxyl-3,7,11-tridecatrienyl]-3-chromen-6-ol, β-caroteno	aromatic derivatives
15	1138	raputindole A	alkaloids
16	1139	raputindole D	alkaloids
17	1646	3-geranylgeranyl, 5-acetoxy-benzofuranone	aromatic derivatives
18	681	(*R*)-MPA-chaetoviridin H	polyketides
19	1644	5-hydroxy-7-(3,7,11,15-tetramethyl-2,6,10,11-hexadecatetraenyl)-2(3*H*)-benzofuranone	aromatic derivatives
20	242	(−)-epigallocatechin-3-*O*-gallate	flavonoids
21	951	1,3,5-trihydroxy-4-methoxy-10-methyl- 2,8-bis(3-methylbut-2-enyl) acridin-9(10*H*)-one	alkaloids

MPA: monophosphoric acid.

4.68 Å (Vina, Figure 3f), 4.02 Å (ChemPLP, Figure 3b) and 4.67 Å (GoldScore, Figure 3d).

Raputindole D

A simulated interaction with raputindole D showed Y268 (Figures 4b, 4d and 4f) pi-pi T-shaped and amide-pi stacked at 4.93 and 4.91 Å in (Vina, Figure 4f), 4.62 and 4.72 Å in (ChemPLP, Figure 4b), and an interaction at 4.75 Å in (GoldScore, Figure 4d). Also, with the Y268 residue, alkyl and pi-alkyl interactions were found at 5.70 Å (Vina, Figure 4f), 5.24 Å (ChemPLP, Figure 4b), and 5.50 Å (GoldScore, Figure 4d). The molecule interacts with N267 through van der Waals forces (Vina and ChemPLP, Figures 4f and 4b, respectively) and pi-pi T-shaped and amide-pi stacked at 6.27 Å (GoldScore, Figure 4d). This was the largest distance found in this study. The interactions with the Q269 residue occurred through pi-pi T-shaped and amide-pi stacked at 6.21 Å (Vina, Figure 4f) and pi-sigma at 4.02 Å (ChemPLP, Figure 4b), and finally, van der Waals forces (GoldScore, Figure 4d) were seen.

The biological activity of PLpro, in conjunction with raputindoles and the docking position of alkaloid class molecules with PLpro, suggests their potential as protease inhibitors.

Pharmacokinetics of NuBBEDB compounds

The MW of raputindole C is 323.5 Da, according to the four programs used. Promiscuity by pan assay interference compounds (PAINS) is negative according to SwissADME and ADMETab 2.0. Table 2 contains the values of the physicochemical descriptors: LogP (pkCSM and ADMETlab 2.0), consensus LogP (DataWarrior and SwissADME), hydrogen acceptors and donors, NRotB and the polar surface relationship. The natural product shows satisfactory absorption with Caco2 > 0.90 (pkCSM). The opposite is seen for ADMETlab 2.0, in which the predicted value is less than –5.15 log cm s^{-1}, which indicates low absorption. However, intestinal absorption, according to both programs, is high: 89.544% for pkCSM and high probability to be above 30% (< 0.3) with ADMETlab 2.0.

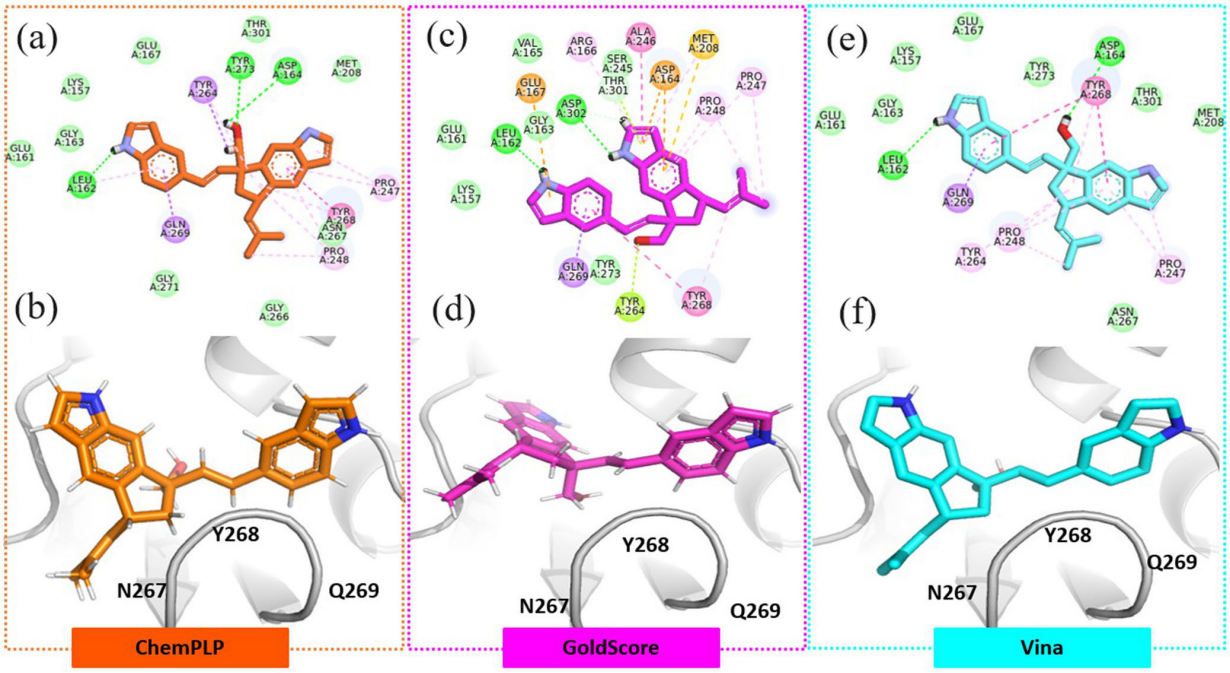

Figure 2. Raputindole C interactions. (a), (c) and (e) DSV interaction analysis maps (b), (d) and (f) docking orientation results between ligands and N267, Y268, and Q269 PLpro residues. Interactions celadon: C–H bond; tea green: van der Waals; moss green: hydrogen bond; lime green: pi lone pair; fuchsia: pi-pi; lavender pink: pi-alkyl; pastel purple: pi sigma; royal purple: amide-pi stacked; carrot orange: pi-anion; terra cotta: unfavorable.

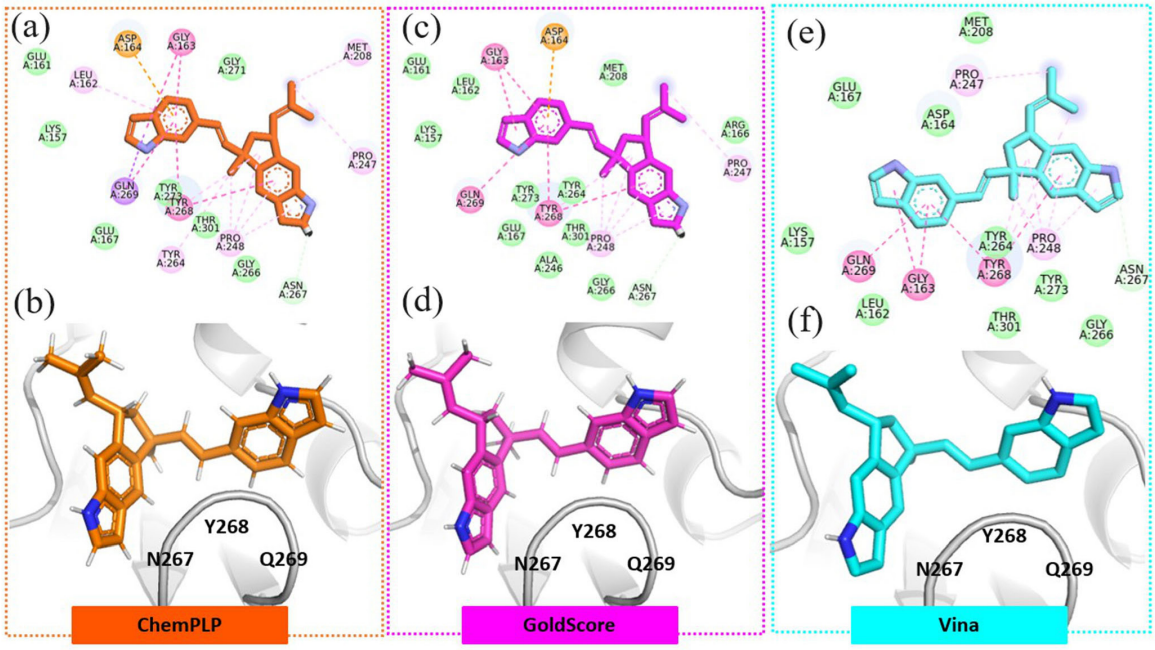

Figure 3. Raputindole A interactions. (a), (c) and (e) DSV interaction analysis maps (b), (d) and (f) docking orientation results between ligands and N267, Y268 and Q269 PLpro residues. Interactions celadon: C–H bond; tea green: van der Waals; moss green: hydrogen bond; lime green: pi lone pair; fuchsia: pi-pi; lavender pink: pi-alkyl; pastel purple: pi sigma; royal purple: amide-pi stacked; carrot orange: pi-anion; terra cotta: unfavorable.

The BBB permeability was negative for both SwisADME and pkCSM (below 0.3) while ADMETlab 2.0 < 0.3 showed high probability of low penetration given by > 1. Raputindole C has a high probability to act as an inhibitor of CYP2C19, CYP2C9 and CYP3A4, and toxicity analysis revealed positive hepatoxicity and respiratory toxicity, while it showed negative mutagenicity and tumorigenicity capacities.

Raputindole A has an MW of 366.5 Da and no PAINS alerts and the overall physical-chemical characteristics are described in Table 3. Worth noting that, it showed high intestinal absorption predicted by pkCSM and

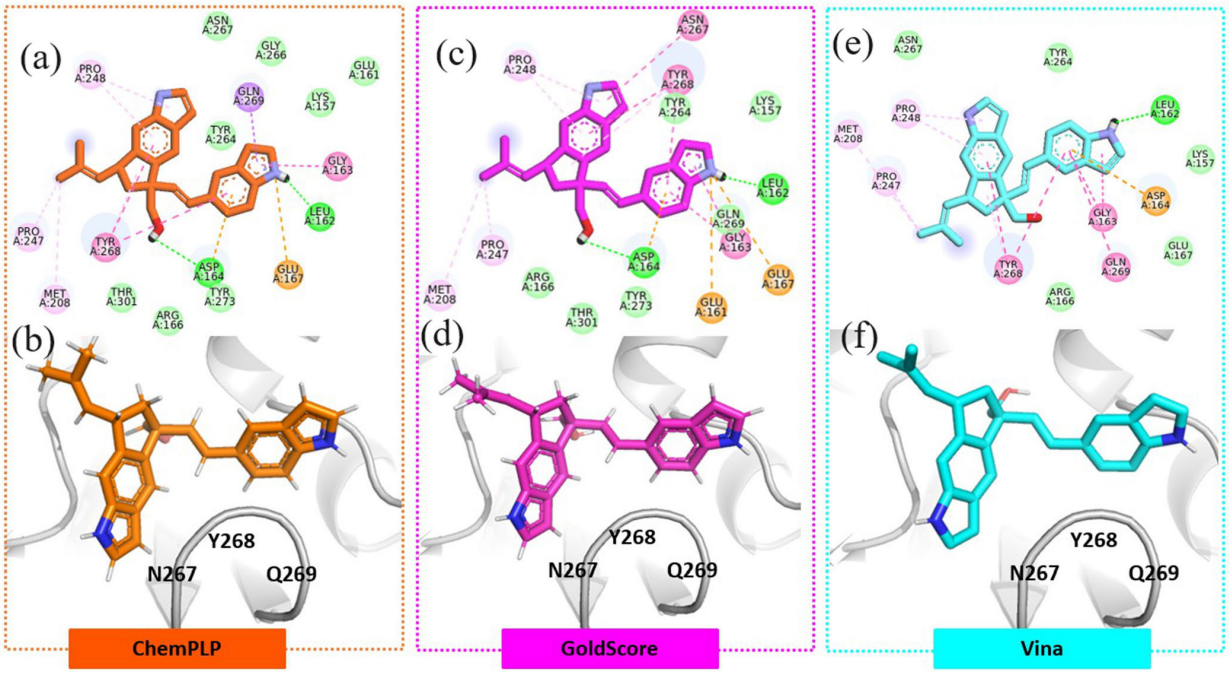

Figure 4. Raputindole D interactions. (a), (c) and (e) DSV interaction analysis maps (b), (d) and (f) docking orientation results between ligands and N267, Y268, and Q269 PLpro residues. Interactions celadon: C–H bond; tea green: van der Waals; moss green: hydrogen bond; lime green: pi lone pair; fuchsia: pi-pi; lavender pink: pi-alkyl; pastel purple: pi sigma; royal purple: amide-pi stacked; carrot orange: pi-anion; terra cotta: unfavorable.

ADMETlab 2.0 and seemed to be both a substrate and inhibitor of PgP. This alkaloid seems to be distributed in the central nervous system via the BBB (pkCSM and ADMETlab 2.0) and like raputindole C, it was hepatotoxic and had positive respiratory toxicity, but it was negative for mutagenic or tumorigenic activities.

In conclusion, raputindole D had the same MW as raputindole C. Like the other molecules, it had no PAINS alerts. Among them, it had the highest intestinal absorption value. Also, it was a Pgp substrate with low BBB permeability and had the same toxicological characteristics as the other two alkaloids. Table 4 summarizes the pharmacokinetic parameters related to its absorption, distribution, metabolism, and toxicity.

NPs tend to be large molecules and therefore have a higher molecular weight.[29] However, the MWs of the alkaloids presented here do not impact their absorption, especially considering the topological polar surface area (TPSA) values, which are much lower than 250 Å. Predictors related to absorption and metabolism are indicators of how promising these substances are for inhibiting SARS-CoV-2 PLpro.

Molecular dynamics and MM/PPBSA analysis

RMSD analysis

We evaluated the stability and dynamics of the protein's interaction with raputindoles A, C, D, as well as GRL0617, by analyzing their RMSD profiles (Figure 5). In a comparative perspective against the simulation results of GRL0617 (Figure 5d), raputindoles A and D demonstrated similar average RMSD values in their interactions with the protein (Figures 5b and 5c). However, PLpro complexed with raputindole C showcased notable fluctuations between the three runs, particularly evident from its peak RMSD value in the first run of the simulation (Figure 5a). When evaluated individually, raputindole D emerged as the most stable compound, while raputindole C displayed the highest dynamism or flexibility.

RMSF analysis

The RMSF provides insights into the positional stability and dynamic behavior of individual residues relative to their average positions. Through RMSF analysis, we assessed the flexibility patterns of the backbone atoms in the native proteins as well as when they are complexed with ligands. The RMSF values for the complexes involving raputindoles A, C, D, and GRL0617, were evaluated to provide insights into their structural stability (Figure 6a).

A thorough analysis was carried out on the BL2 region, which covers residues G266 to G271 (depicted in Figure 6b). The findings revealed distinct RMSF values within this region. Notably, raputindole A exhibited the highest RMSF value, measuring at 2.367 Å, whereas the lowest value of 0.742 Å was observed for the same compound. For raputindole C, its RMSF peaked at 2.569 Å, with a minimum

Table 2. Pharmacokinetic parameters predicted by DataWarrior, pkCSM, SwissADME and ADMETlab 2.0 for raputindole C

Physicochemical properties	DataWarrior	pkCSM	SwissADME	ADMETlab2.0
MW / Da	382.505	382.507	382.5	382.2
PAINS	–	–	negative	negative
cLogP	5.7925	–	5.13	–
LogP	–	6.0462	–	5.806
H-Acceptors	3	1	1	3
H-Donors	3	3	3	3
NRotB	–	4	4	4
Polar surface area / Å	51.81	–	–	–
Surface area / Å	–	170.329	–	–
Topological polar surface area / Å	–		51.81	51.81
Absorption				
Caco2 permeability	–	0.974	–	–5.315
Intestinal absorption (human)	–	89.544	–	0.005
GI absorption	–	–	high	–
P-glycoprotein substrate	–	positive	positive	0.997
P-glycoprotein inhibitor	–	–	–	0.991
P-glycoprotein I inhibitor	–	positive	–	–
P-glycoprotein II inhibitor	–	positive	–	–
Distribution				
BBB permeability	–	–0.068	negative	0.132
Metabolism				
CYP1A2 inhibitor	–	–	negative	0.886
CYP2C19 inhibitor	–	–	positive	0.948
CYP2C9 inhibitor	–	–	positive	0.894
CYP2D6 inhibitor	–	–	negative	0.895
CYP3A4 inhibitor	–	–	positive	0.925
Toxicity				
Hepatotoxicity	–	positive	–	–
Mutagenic	negative	–	–	–
Tumorigenic	negative	–	–	–
Respiratory toxicity	–	–	–	0.967

MW: molecular weight; PAINS: pan-assay interference compounds; cLogP: calculated log partition coefficient; logP: logarithm of the partition coefficient between octanol and water; NRotB: number of rotatable bonds; Caco2: Caco-2 permeability; GI: gastrointestinal absorption; BBB: blood-brain barrier; CYPs: cytochrome P450 enzymes.

of 0.75 Å. Similarly, raputindole D displayed a maximum RMSF of 1.814 Å and a minimum of 0.761 Å. In the case of GRL0617, its RMSF values ranged from 1.424 Å at its maximum to 0.719 Å at its minimum. Intriguingly, within the context of the BL2 region, raputindole D displayed the least flexibility among the compounds, as indicated by its smallest RMSF value. This suggests that the BL2 region remains most stable in the presence of raputindole D. On the other hand, raputindole A revealed the highest flexibility in the BL2 region among the three. Raputindole C showcased an intermediate level of flexibility for this specific region.

A more detailed analysis was undertaken for residues N267, Y268, and Q269, which are part of the BL2 region and hotspots for PLpro inhibition. These values provide insights into the localized flexibilities of these specific residues across different ligand environments.

Hydrogen bonds analysis

The number of hydrogen bonds formed in a molecular complex can provide insights into its stability and interaction dynamics. In the case of raputindole C, the average number of hydrogen bonds formed was 3604, 4030, and 7648, respectively, for each run (Figure 7a). This suggests a moderate level of interaction, potentially contributing to the stability of the complex. Raputindole A

Table 3. Pharmacokinetic parameters predicted by DataWarrior, pkCSM, SwissADME and ADMETlab 2.0 for raputindole A

Physicochemical properties	DataWarrior	pkCSM	SwissADME	ADMETlab2.0
MW / Da	366.506	366.508	366.5	366.21
PAINS	–	–	negative	negative
cLogP	6.7192	–	5.99	–
LogP	–	7.0738	–	6.403
H-Acceptors	2	0	0	2
H-Donors	2	2	2	2
NRotB	–	3	3	3
Polar surface area / Å	31.58	–	–	–
Surface area / Å	–	165.535	–	–
Topological polar surface area / Å	–	–	31.58	31.58
Absorption				
Caco2 permeability	–	0.974	–	–5.163
Intestinal absorption (human)	–	89.66	–	0.005
GI absorption	–	–	low	–
P-glycoprotein substrate		positive	positive	0.118
P-glycoprotein inhibitor	–	–	–	0.996
P-glycoprotein I inhibitor	–	positive	–	–
P-glycoprotein II inhibitor	–	positive	–	–
Distribution				
BBB permeability	–	0.72	negative	0.053
Metabolism				
CYP1A2 inhibitor	–	–	positive	0.918
CYP2C19 inhibitor	–	–	positive	0.953
CYP2C9 inhibitor	–	–	positive	0.926
CYP2D6 inhibitor	–	–	negative	0.712
CYP3A4 inhibitor	–	–	positive	0.95
Toxicity				
Hepatotoxicity	–	positive	–	–
Mutagenic	negative	–	–	–
Tumorigenic	negative	–	–	–
Respiratory toxicity	–	–	–	0.94

MW: molecular weight; PAINS: pan-assay interference compounds; cLogP: calculated log partition coefficient; logP: logarithm of the partition coefficient between octanol and water; NRotB: number of rotatable bonds; Caco2: Caco-2 permeability; GI: gastrointestinal absorption; BBB: blood-brain barrier; CYPs: cytochrome P450 enzymes.

showed an average of 445, 989, 488 hydrogen bonds for each run (Figure 7b). This lower number indicates fewer interactions, which might suggest a more dynamic or less stable interaction pattern in comparison to the other datasets. Interestingly, the complex in raputindole D had the highest average number of hydrogen bonds, with a value of 8508, 7440, 8175 for each run (Figure 7c). This indicates robust interaction, possibly resulting in a more stable complex compared to the other two. Compared to the GRL0617 results, which were 7948, 7997, and 7917 respectively, from runs 1 to 3, raputindole D exhibited a higher number of hydrogen bonds.

Overall, these results offer a comparative perspective on the stability of the complexes based on their hydrogen bonding patterns during the simulation.

MM/PBSA analysis

The binding free energies of PLpro-ligand complexes with raputindoles C, A, D, and GRL0617 were computed using the MM/PBSA method. The calculated energy components and the resulting binding energies are summarized in Table 5.

Despite GRL0617, raputindole A complex demonstrated the most favorable binding energy, followed by raputindole D, suggesting the strongest interaction with

Table 4. Pharmacokinetic parameters predicted by DataWarrior, pkCSM, SwissADME and ADMETlab 2.0 for raputindole D

Physicochemical properties	DataWarrior	pkCSM	SwissADME	ADMETlab2.0
MW / Da	382.505	382.507	382.5	382.2
PAINS	–	–	negative	negative
cLogP	5.7925	–	5.16	–
LogP	–	6.0462	–	5.455
H-Acceptors	3	1	1	3
H-Donors	3	3	3	3
NRotB		4	4	4
Polar surface area / Å	51.81	–	–	–
Surface area / Å	–	170.329	–	–
Topological polar surface area / Å			51.81	51.81
Absorption				
Caco2 permeability	–	1.017	–	-5.507
Intestinal absorption (human)	–	92.617		0.006
GI absorption	–	-	high	–
P-glycoprotein substrate		positive	positive	0.994
P-glycoprotein inhibitor	–	–		1
P-glycoprotein I inhibitor	–	positive	–	–
P-glycoprotein II inhibitor	–	positive	–	–
Distribution				
BBB permeability	–	–0.061	negative	0.199
Metabolism				
CYP1A2 inhibitor	–	–	negative	0.892
CYP2C19 inhibitor	–	–	positive	0.948
CYP2C9 inhibitor	–	–	positive	0.914
CYP2D6 inhibitor	–	–	negative	0.837
CYP3A4 inhibitor	–	–	positive	0.921
Toxicity				
Hepatotoxicity	–	positive	–	–
Mutagenic	negative	–	–	–
Tumorigenic	negative	–	–	–
Respiratory toxicity	–	–	–	0.957

MW: molecular weight; PAINS: pan-assay interference compounds; cLogP: calculated log partition coefficient; logP: logarithm of the partition coefficient between octanol and water; NRotB: number of rotatable bonds; Caco2: Caco-2 permeability; GI: gastrointestinal absorption; BBB: blood-brain barrier; CYPs: cytochrome P450 enzymes.

PLpro. This is consistent with the higher negative values observed for both van der Waals and electrostatic energies. Conversely, raputindole C had the least favorable binding energy, indicating the weakest interaction with PLpro.

Discussion

PLpro is a protease crucial for multiple proteolytic functions and for processing viral polyproteins, viral maturation, and replication.[47] Functionally, SARS-CoV-2 PLpro is a potential drug target against COVID-19.[48] Natural product-derived molecules are attractive as drug targets due to their ability to undergo rapid safety evaluation.[49] In this study, we present an *in silico* investigation of NuBBEDB molecules and found that raputindoles exhibit inhibitory potential against SARS-CoV-2 PLpro.

Molecular docking and virtual screening

Figure 1 shows the redocking performed using the GRL0617 inhibitor found in PDB 7JRN,[50] which was used here to validate our method. Redocking presented both docking energies and interactions between the residues of interest, especially Y268, which is similar to that observed

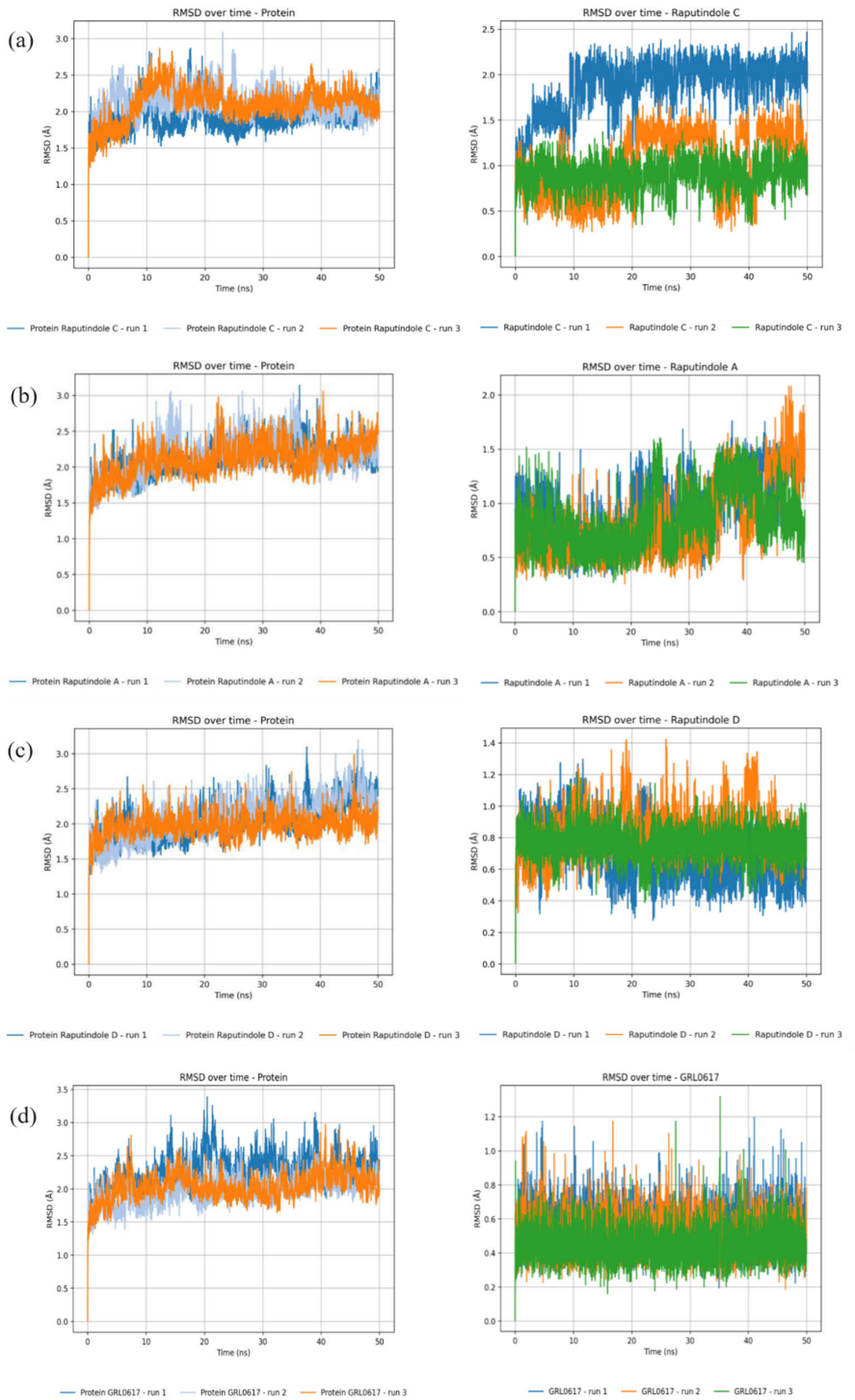

Figure 5. Comparative root mean square deviations (RMSD) of raputindoles and GRL0617 interactions with proteins. (a) RMSD of PLpro receptor, and raputindole C, over the simulation time. (b) RMSD of PLpro receptor, and raputindole A. (c) RMSD of PLpro receptor, and raputindole D. (d) RMSD of PLpro receptor, and GRL0617.

in the crystal structure. Also, our *in silico* methodology is in line with our previous studies,[11] especially for the *in vitro* description of the flavonoid inhibitory potential.

Flavonoids were, together with alkaloids, at the top of our ranking (Table 1) and these findings are supported by previous *in vitro* studies.[11] It is well known that NPs play a key role in the pharmacological industry, as a source of novel and unexplored molecular core, which is of utmost interest during the development of new drug processes. Our virtual screening results identified natural alkaloids as potential inhibitors of the SARS-CoV-2 PLpro. Alkaloids are a class with at least one nitrogen as a

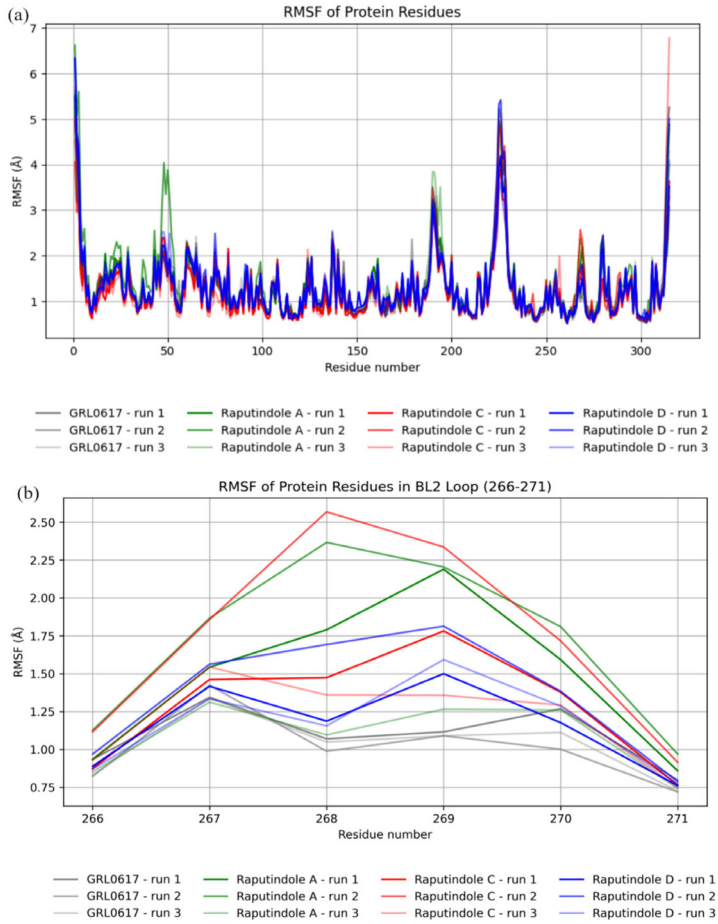

Figure 6. (a) RMSF values illustrating the positional stability and dynamic behavior of residues when complexed with raputindoles A, C, D, and GRL0617; (b) focused RMSF analysis of the Beta-Loop-2 (BL2) region (G266-G271). Residues N267, Y268, and Q269, which are critical for PLpro inhibition, show varied flexibilities across different ligand environments.

heteroatom, usually in a heterocyclic ring, known to have broad pharmacological activity and produce pronounced physiological responses, making them a powerful candidate to treat viral pathologies. Not surprisingly, they have been used as prototypes for the development of synthetic antiviral drugs.[45]

Currently, more than 8,000 natural compounds are classified as alkaloids, among them 288 are found in NuBBEDB.[19,51] Among alkaloids, our results show that indole raputindoles, which were first isolated in 2011 from samples of *Raputia simulans* from Brazilian Amazon Forest[20] are the most interesting candidates to PLpro inhibition. Indoles are active molecules that can be modified to generate a huge variety of derivatives, which makes this chemical class of great importance in pharma industry.[52,53] There are many studies about the medicinal applications of indoles, but descriptions of these molecules' interactions with PLpro are still incipient.[54] Alkaloids have already been reported as potential viral inhibitors,[54,55] but we describe for the first time the potential of indole raputindoles as SARS- CoV-2 PLpro inhibitors.

Analysis of the interactions between rapuntidoles and the PLpro enzyme

In all raputindoles simulations, we observed the formation of hydrogen bonds with PLpro residues (Figures 2, 3, and 4). The bridges formed indicate that raputindole D forms a greater amount of interactions when compared with the found with the inhibitor GRL0617.[44] The most promising was the hydrogen bond that occurs in all simulations with residue Y268, which has been identified as a critical residue for protease function. Hydrogen interactions between PLpro Y268 and NPs have already been found and described for flavonoids, in which inhibition of enzymatic activity was observed.[11]

The pi-pi T-shaped interactions found in our simulations are considered a broad category of noncovalent interactions.[56] In the pi-pi T-shaped interaction there is an electron cloud interaction between two aromatic groups. In a T-shaped, there is a side electron cloud of a ring and an electron cloud of another ring.[56,57] Also, in noncovalent interactions we observed the pi-alkyl, alkyl, and pi-sigma interactions,

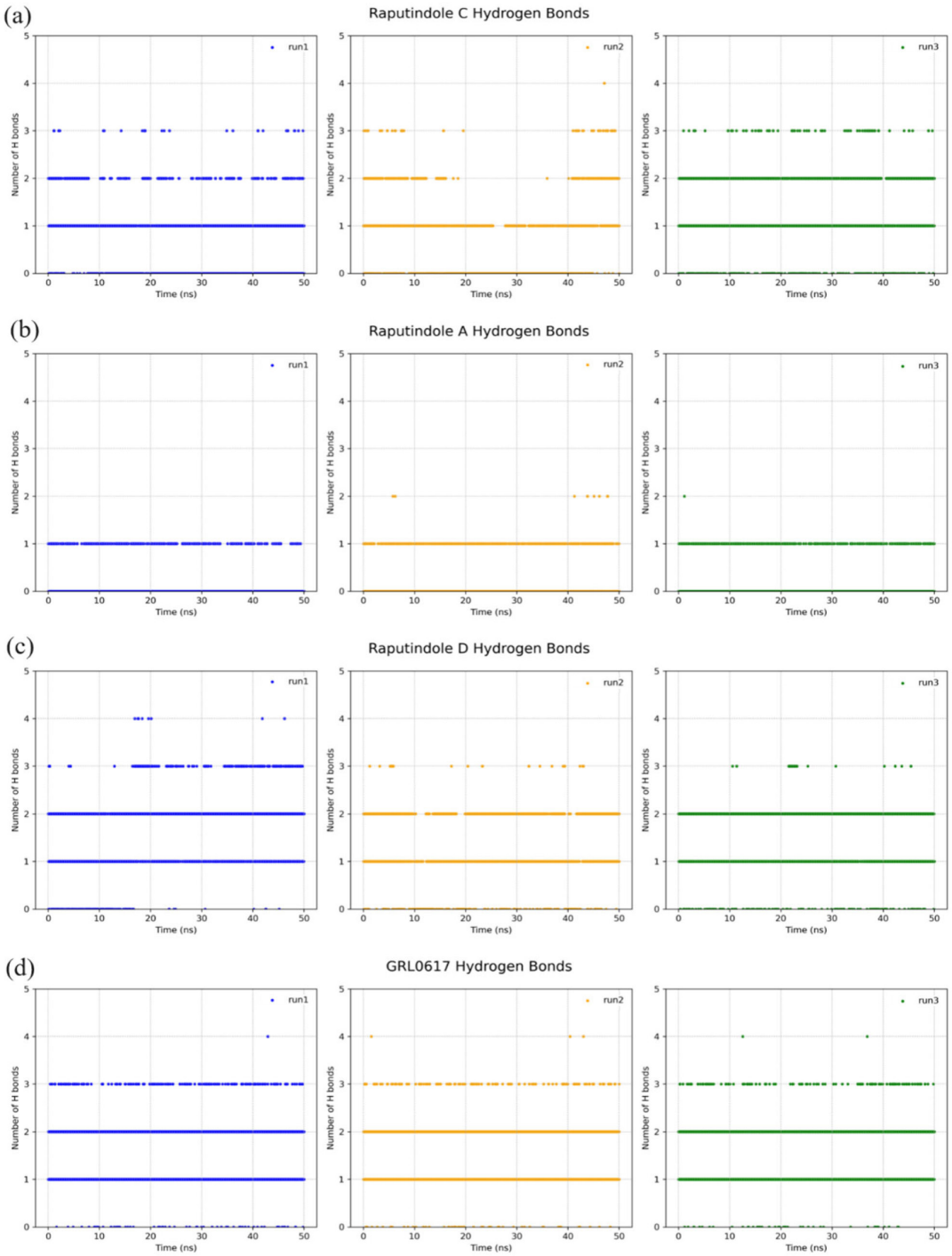

Figure 7. Comparative analysis of the average number of hydrogen bonds formed in three different raputindole complexes. (a) Raputindole C complex with 3604, 4030, and 7648 hydrogen bonds; (b) raputindole A complex showing 445, 989, 48 hydrogen bonds; (c) raputindole D complex exhibiting the highest number of hydrogen bonds 8508, 7440, 8175. (d) GRL0617 with 7948, 7997, and 7917 hydrogen bonds.

where an electron cloud interacts with an aromatic group while an electron group interacts with an alkyl group.[57] Considering the hall of noncovalent interactions simulated in our study, pi-stacked amide interactions are known to result in an amplification of hydrogen bond energy.[58] All interactions are hydrophobic and play a significant role as enzyme inhibitors.[11,56,57] The observed van der Waals interactions indicate the inhibitory potential of this NP protein.[59]

Physicochemical properties of raputindoles

Drug-likeness properties play a crucial role in antiviral drug development. Currently, several drugs fall into the broad

Table 5. Binding free energy calculations of PLpro-ligand complexes using MM/PBSA

	Energy type / (kcal mol^{-1})		
	Raputindole A-run 1	Raputindole A-run 2	Raputindole A-run 3
Van der Waals energy	–39.76 ± 4.51	–37.60 ± 6.62	–43.03 ± 3.11
Electrostatic energy	–8.39 ± 3.95	–10.01 ± 3.00	–13.38 ± 3.62
Polar solvation energy	34.08 ± 6.65	32.40 ± 4.98	35.41 ± 5.66
Binding energy	–14.07 ± 8.95	–21.24 ± 6.80	–21.00 ± 7.40
	Raputindole D-run 1	Raputindole D-run 2	Raputindole D-run 3
Van der Waals energy	–39.02 ± 3.98	–35.37 ± 4.35	–38.04 ± 3.12
Electrostatic energy	–17.96 ± 4.20	–18.89 ± 5.05	–21.00 ± 3.78
Polar solvation energy	43.10 ± 5.97	40.84 ± 6.38	41.34 ± 5.25
Binding energy	–13.88 ± 8.31	–13.42 ± 9.23	–17.70 ± 7.18
	Raputindole C-run 1	Raputindole C-run 2	Raputindole C-run 3
Van der Waals energy	–25.79 ± 4.78	–25.93 ± 7.42	–39.02 ± 3.98
Electrostatic energy	–8.07 ± 4.19	–10.87 ± 4.47	–17.96 ± 4.20
Polar solvation energy	26.81 ± 4.50	25.54 ± 9.26	43.10 ± 5.97
Binding energy	–7.05 ± 7.79	–11.26 ± 12.68	–13.88 ± 8.31
	GRL0617-run 1	GRL0617-run 2	GRL0617-run 3
Van der Waals energy	–35.71 ± 1.99	–35.89 ± 2.02	–35.90 ± 2.17
Electrostatic energy	–18.17 ± 4.61	–17.75 ± 4.17	–17.62 ± 3.73
Polar solvation energy	32.29 ± 5.32	32.40 ± 4.98	32.07 ± 4.76
Binding energy	–21.59 ± 7.32	–21.24 ± 6.80	–21.45 ± 6.42

druggable space determined by Beyonde Rule of 5 (bRO5). Among them is azithromycin, a well-known antibiotic with MW = 749 Da and protease inhibitors simeprevir and atazanavir, which also have MW greater than 700 Da.[60] Likewise, the physical-chemical characteristics of the NPs screened in this work go beyond the traditional Lipinski's rule of 5.[61] Therefore, the bRO5 druggable space allows larger and more complex substances, such as NPs, to be considered as drugs. For this reason, we based on the bRO5 criteria to analyze those molecules that best interacted with the SARS-CoV-2 PLpro.[62]

The bioavailability of a drug is intrinsically connected to its ability to be absorbed through the intestinal epithelium and reach the systemic circulation.[63] Among other absorption factors, P-glycoprotein is a type of ATPase that acts in the efflux of these substances, which can interfere with the efficiency of pharmacological activity.[64] Our results show that rapuntindoles A, B and C present satisfactory intestinal absorption, as calculated by pkCSM and ADMETlab 2.0. In addition, they are Pgp substrates and Pgp I and II inhibitors as well, which reinforce the epithelial transit to the intestinal lumen. The NPs in their raw structure may not show sustainable ADMET results. Therefore, the optimization of structure through the identification of hits and the elaboration of leads can be an alternative in the functionalization of structure and production of successful drugs.[65,66] Through the predictions of physicochemical characteristics, we identified that the three raputindoles do not show mutagenicity or tumorigenic potential (Tables 2, 3 and 4). However, they can have hepatotoxic effects and trigger respiratory toxicity. Manifestations of pulmonary drug toxicity may occur because of the use of certain anti-inflammatories and antimicrobials for weeks, being detected by imaging tests or histopathological findings.[67] Despite these characteristics, several studies[68-70] discuss the antiviral activity of the alkaloids, which is reinforced by technological advances and the possibility of optimizing the structure of the raputindoles studied here.

Molecular dynamics and MM/PBSA analysis

The molecular dynamics analyses indicate the stability of the formed complexes, particularly highlighting the stability of raputindole D in comparison to GRL0617, a well-known inhibitor of PLpro.[71] This conclusion is drawn from the observed RMSD values. This is based on the premise that structures with consistently low RMSD values throughout the simulation are indicative of a likely interaction.[72,73]

The RMSF results suggest that, despite slight variations among them, raputindoles tend to maintain protein

stability, particularly in the BL2 region, which is critical for inhibiting Plpro function.[74]

Hydrogen bond interactions, essential for upholding the complex's structure, are observed to be consistently stable.[44] This observation is especially pronounced in the case of raputindole D, which, in two out of the three runs, forms a greater number of hydrogen bonds compared to those identified in GRL0617. Both the results from hydrogen bond interactions and MM/PBSA analyses indicate that the interaction energies of the raputindoles are favorable and remain consistent with residues of interest N267, Y268, and Q269.[73]

While each ligand displays distinct properties, raputindole D consistently stands out as a potential candidate due to its favorable interactions, especially in stabilizing the pivotal BL2 loop region.[75] This suggests potential implications for its efficiency as an inhibitor and underscores the need for further experimental validations. In reflecting on our research, it is important to acknowledge the potential importance of other classes of molecules that were not the primary focus of our study, such as phenylethanoid glycosides (PGs), chalcones, and aromatic derivates. These molecules, although outside our primary scope of investigation, could potentially offer additional or complementary pathways to inhibit SARS-CoV-2. Notably, PGs have been reported to possess potential as selective inhibitors of SARS-CoV-2 PLpro.[76] We strongly believe in the need for a comprehensive approach to COVID-19 research, and as such, encourage further investigation into these compounds to fully realize their potential.

Conclusions

In summary, this study suggests that NPs, especially indole raputindoles that interact with the BL2 loop region of PLpro have the potential to act as SARS-CoV-2 inhibitors. Although these results were obtained from *in silico* analysis, the formation of the simulated interactions allows us to predict the inhibitory potential of this NP compound. Our analysis revealed that raputindole C displayed the highest stability with the protein, as evidenced by its lowest RMSD and RMSF values, suggesting consistent positioning and structural stability. A detailed study of the BL2 region pinpointed raputindole D as the most effective in stabilizing this crucial segment. The presence of significant hydrogen bonds further emphasizes the stability of these complexes. Collectively, the findings underline the potential of raputindoles, particularly D, as promising candidates for SARS-CoV-2 therapeutic interventions, given their favorable interactions with PLpro.

Acknowledgments

The authors would like to thank the Universidade Federal do Rio de Janeiro for the scientific and technical assistance they provided. They also would like to thank Coordenação de Aperfeiçoamento de Pessoal de Nível Superior (CAPES), Fundação Carlos Chagas Filho de Amparo à Pesquisa do Estado do Rio de Janeiro (FAPERJ) and Conselho Nacional de Desenvolvimento Científico e Tecnológico (CNPq) for the fomentation provided.

References

1. Cucinotta, D.; Vanelli, M.; *Acta Biomed.* **2020**, *91*, 157. [Crossref]
2. World Health Organization; *WHO Coronavirus (COVID-19) Dashboard*, https://covid19.who.int/table, accessed in August 2023.
3. Fernández-de-las-Peñas, C.; Palacios-Ceña, D.; Gómez-Mayordomo, V.; Florencio, L. L.; Cuadrado, M. L.; Plaza-Manzano, G.; Navarro-Santana, M.; *Eur. J. Intern. Med.* **2021**, *92*, 55. [Crossref]
4. Levin, E. G.; Lustig, Y.; Cohen, C.; Fluss, R.; Indenbaum, V.; Amit, S.; Doolman, R.; Asraf, K.; Mendelson, E.; Ziv, A.; Rubin, C.; Freedman, L.; Kreiss, Y.; Regev-Yochay, G.; *N. Engl. J. Med.* **2021**, *385*, e84. [Crossref]
5. Sockrider, M.; Krishnan, J. A.; *Am. J. Respir. Crit. Care Med.* **2021**, *203*, P16. [Crossref]
6. Gil, C.; Ginex, T.; Maestro, I.; Nozal, V.; Barrado-Gil, L.; Cuesta-Geijo, M. Á.; Urquiza, J.; Ramírez, D.; Alonso, C.; Campillo, N. E.; Martinez, A.; *J. Med. Chem.* **2020**, *63*, 12359. [Crossref]
7. Kumar, A.; Parashar, R.; Kumar, S.; Faiq, M. A.; Kumari, C.; Kulandhasamy, M.; Narayan, R. K.; Jha, R. K.; Singh, H. N.; Prasoon, P.; Pandey, S. N.; Kant, K.; *J. Med. Virol.* **2022**, *94*, 1300. [Crossref]
8. Shin, D.; Mukherjee, R.; Grewe, D.; Bojkova, D.; Baek, K.; Bhattacharya, A.; Schulz, L.; Widera, M.; Mehdipour, A. R.; Tascher, G.; Geurink, P. P.; Wilhelm, A.; van der Heden van Noort, G. J.; Ovaa, H.; Müller, S.; Knobeloch, K.-P.; Rajalingam, K.; Schulman, B. A.; Cinatl, J.; Hummer, G.; Ciesek, S.; Dikic, I.; *Nature* **2020**, *587*, 657. [Crossref]
9. Dashdorj, N.; Wirz, O. F.; Röltgen, K.; Haraguchi, E.; Buzzanco, A. S.; Sibai, M.; Wang, H.; Miller, J. A.; Solis, D.; Sahoo, M. K.; Arunachalam, P. S.; Lee, A. S.; Shah, M.; Liu, J. J. Y.; Byambabaatar, S.; Bat-Ulzii, P.; Enkhbat, A.; Batbold, E.; Zulkhuu, D.; Ochirsum, B.; Khurelsukh, T.; Dalantai, G.; Burged, N.; Baatarsuren, U.; Ariungerel, N.; Oidovsambuu, O.; Bungert, A.; Genden, Z.; Yagaanbuyant, D.; Mordorj, A.; Pulendran, B.; Chinthrajah, S.; Nadeau, K. C.; Jardetzky, T. S.; Wilbur, J. L.; Wohlstadter, J. N.; Sigal, G.; Pinsky, B. A.; Boyd, S. D.; Dashdorj, N.; *Cell Host Microbe* **2021**, *29*, 1738. [Crossref]

10. Krichel, B.; Falke, S.; Hilgenfeld, R.; Redecke, L.; Uetrecht, C.; *Biochem. J.* **2020**, *477*, 1009. [Crossref]
11. Leal, C. M.; Leitão, S. G.; Sausset, R.; L.; Mendonça, S. C.; Nascimento, P. H. A.; Cheohen, C. F. A. R.; Esteves, M. E. A.; da Silva, M. L.; Gondim, T. S.; Monteiro, M. E. S.; Tucci, A. R.; Rodrigues, N. F.; Siqueira, M. M.; Miranda, M. D.; Costa, F. N.; Simas, R. C.; Leitão, G. G.; *Rev. Bras. Farmacogn.* **2021**, *31*, 658. [Crossref]
12. Luan, J.; Jin, X.; Lu, Y.; Zhang, L.; *J. Med. Virol.* **2020**, *92*, 1649. [Crossref]
13. Sook Mun, C.; Yong Hui, L.; Cong Sing, L.; Karunakaran, R.; Ravichandran, V.; *Saudi J. Biol. Sci.* **2022**, *29*, 103458. [Crossref]
14. Yue, S.; Li, Z.; Lin, Y.; Yang, Y.; Yuan, M.; Pan, Z.; Hu, L.; Gao, L.; Zhou, J.; Tang, J.; Wang, Y.; Tian, Q.; Hao, Y.; Wang, J.; Huang, Q.; Xu, L.; Zhu, B.; Liu, P.; Deng, K.; Wang, L.; Ye, L.; Chen, X.; *Front. Immunol.* **2021**, *12*, 751584. [Crossref]
15. Zhong, L.; Zhao, Z.; Peng, X.; Zou, J.; Yang, S.; *Precis. Clin. Med.* **2022**, *5*, pbac024. [Crossref]
16. Boozari, M.; Hosseinzadeh, H.; *Phyther. Res.* **2021**, *35*, 864. [Crossref]
17. Ekiert, H. M.; Szopa, A.; *Molecules* **2020**, *25*, 5769. [Crossref]
18. Valli, M.; Russo, H. M.; Bolzani, V. S.; *An. Acad. Bras. Ciênc.* **2018**, *90*, 763. [Crossref]
19. Pilon, A. C.; Valli, M.; Dametto, A. C.; Pinto, M. E. F.; Freire, R. T.; Castro-Gamboa, I.; Andricopulo, A. D.; Bolzani, V. S.; *Sci. Rep.* **2017**, *7*, 7215. [Crossref]
20. Rosas, L. V.; Veiga, T. A. M.; Fernandes, J. B.; Vieira, P. C.; da Silva, M. F. G. F.; *J. Braz. Chem. Soc.* **2011**, *22*, 1346. [Crossref]
21. Trot, O.; Olson, A. J.; *J. Comput. Chem.* **2010**, *31*, 455. [Crossref]
22. Jones, G.; Willett, P.; Glen, R. C.; Leach, A. R.; Taylor, R.; *J. Mol. Biol.* **1997**, *267*, 727. [Crossref]
23. Olsson, M. H. M.; Søndergaard, C. R.; Rostkowski, M.; Jensen, J. H.; *J. Chem. Theory Comput.* **2011**, *7*, 525. [Crossref]
24. Dolinsky, T. J.; Czodrowski, P.; Li, H.; Nielsen, J. E.; Jensen, J. H.; Klebe, G.; Baker, N. A.; *Nucleic Acids Res.* **2007**, *35*, 522. [Crossref]
25. Pettersen, E. F.; Goddard, T. D.; Huang, C. C.; Couch, G. S.; Greenblatt, D. M.; Meng, E. C.; Ferrin, T. E.; *J. Comput. Chem.* **2004**, *25*, 1605. [Crossref]
26. *BIOVIA, Discovery Studio Visualizer*, v. 4.5, Dassault Systèmes, San Diego, USA, 2022.
27. Hu, Y.; Bajorath, J.; *Eur. J. Med. Chem.* **2014**, *76*, 427. [Crossref]
28. Daina, A.; Michielin, O.; Zoete, V.; *Sci. Rep.* **2017**, *7*, 42717. [Crossref]
29. Pires, D. E. V.; Blundell, T. L.; Ascher, D. B.; *J. Med. Chem.* **2015**, *58*, 4066. [Crossref]
30. Sander, T.; Freyss, J.; Von Korff, M.; Rufener, C.; *J. Chem. Inf. Model.* **2015**, *55*, 460. [Crossref]
31. Xiong, G.; Wu, Z.; Yi, J.; Fu, L.; Yang, Z.; Hsieh, C.; Yin, M.; Zeng, X.; Wu, C.; Lu, A.; Chen, X.; Hou, T.; Cao, D.; *Nucleic Acids Res.* **2021**, *49*, W5. [Crossref]
32. Paissoni, C.; Spiliotopoulos, D.; Musco, G.; Spitaleri, A.; *Comput. Phys. Commun.* **2015**, *186*, 105. [Crossref]
33. Lindahl, E.; Hess, B.; van der Spoel, D.; *J. Mol. Model.* **2001**, *7*, 306. [Crossref]
34. Huang, J.; MacKerell Jr., A. D.; *J. Comput. Chem.* **2013**, *34*, 2135. [Crossref]
35. Kim, M.; Thompson, C. T.; *Brain Lang.* **2004**, *88*, 1. [Crossref]
36. Vanommeslaeghe, K.; Hatcher, E.; Acharya, C.; Kundu, S.; Zhong, S.; Shim, J.; Darian, E.; Guvench, O.; Lopes, P.; Vorobyov, I.; Mackerell Jr., A. D.; *J. Comput. Chem.* **2010**, *31*, 671. [Crossref]
37. Yu, W.; He, X.; Vanommeslaeghe, K.; MacKerell Jr., A. D.; *J. Comput. Chem.* **2012**, *33*, 2451. [Crossref]
38. Darden, T.; York, D.; Pedersen, L.; *J. Chem. Phys.* **1993**, *98*, 10089. [Crossref]
39. Valdés-Tresanco, M. S.; Valdés-Tresanco, M. E.; Valiente, P. A.; Moreno, E.; *J. Chem. Theory Comput.* **2021**, *17*, 6281. [Crossref]
40. Miller, B. R.; McGee, T. D.; Swails, J. M.; Homeyer, N.; Gohlke, H.; Roitberg, A. E.; *J. Chem. Theory Comput.* **2012**, *8*, 3314. [Crossref]
41. Kumari, R.; Kumar, R.; Lynn, A.; *J. Chem. Inf. Model.* **2014**, *54*, 1951. [Crossref]
42. Hunter, J. D.; *Comput. Sci. Eng.* **2007**, *9*, 90. [Crossref]
43. Elseginy, S. A.; Anwar, M. M.; *RSC Adv.* **2021**, *11*, 38616. [Crossref]
44. Fu, Z.; Huang, B.; Tang, J.; Liu, S.; Liu, M.; Ye, Y.; Liu, Z.; Xiong, Y.; Zhu, W.; Cao, D.; Li, J.; Niu, X.; Zhou, H.; Zhao, Y. J.; Zhang, G.; Huang, H.; *Nat. Commun.* **2021**, *12*, 488. [Crossref]
45. Fielding, B. C.; Bezerra Filho, C. S. M.; Ismail, N. S. M.; de Sousa, D. P.; *Molecules* **2020**, *25*, 5496. [Crossref]
46. Mouffouk, C.; Mouffouk, S.; Mouffouk, S.; Hambaba, L.; Haba, H.; *Eur. J. Pharmacol.* **2021**, *891*, 173759. [Crossref]
47. Osipiuk, J.; Azizi, S. A.; Dvorkin, S.; Endres, M.; Jedrzejczak, R.; Jones, K. A.; Kang, S.; Kathayat, R. S.; Kim, Y.; Lisnyak, V. G.; Maki, S. L.; Nicolaescu, V.; Taylor, C. A.; Tesar, C.; Zhang, Y. A.; Zhou, Z.; Randall, G.; Michalska, K.; Snyder, S. A.; Dickinson, B. C.; Joachimiak, A.; *Nat. Commun.* **2021**, *12*, 743. [Crossref]
48. Calleja, D. J.; Lessene, G.; Komander, D.; *Front. Chem.* **2022**, *10*, 876212. [Crossref]
49. Rehman, Z.; Umair, M.; Ikram, A.; Salman, M.; Haider, S. A.; Ammar, M.; *ChemRxiv* **2021**. [Crossref]
50. Ma, C.; Sacco, M. D.; Xia, Z.; Lambrinidis, G.; Townsend, J. A.; Hu, Y.; Meng, X.; Szeto, T.; Ba, M.; Zhang, X.; Gongora, M.; Zhang, F.; Marty, M. T.; Xiang, Y.; Kolocouris, A.; Chen, Y.; Wang, J.; *ACS Cent. Sci.* **2021**, *7*, 1245. [Crossref]

51. Kishimoto, S.; Sato, M.; Tsunematsu, Y.; Watanabe, K.; *Molecules* **2016**, *21*, 1078. [Crossref]
52. Keskin, S.; Doğan, Ş. D.; Gündüz, M. G.; Aleksic, I.; Vojnovic, S.; Lazic, J.; Nikodinovic-Runic, J.; *J. Mol. Struct.* **2022**, *1270*, 133936. [Crossref]
53. Bhardwaj, V. K.; Singh, R.; Sharma, J.; Rajendran, V.; Purohit, R.; Kumar, S.; *J. Biomol. Struct. Dyn.* **2020**, *39*, 3449. [Crossref]
54. Giampieri, M.; Balbi, A.; Mazzei, M.; La Colla, P.; Ibba, C.; Loddo, R.; *Antiviral Res.* **2009**, *83*, 179. [Crossref]
55. Severino, R. P.; Guido, R. V. C.; Marques, E. F.; Brömme, D.; da Silva, M. F. D. G. F.; Fernandes, J. B.; Andricopulo, A. D.; Vieira, P. C.; *Bioorganic Med. Chem.* **2011**, *19*, 1477. [Crossref]
56. Alencar, W. L. M.; da Silva Arouche, T.; Gomes Neto, A. F.; Ramalho, T. C.; de Carvalho Jr., R. N.; Chaves Neto, A. M. J.; *Sci. Rep.* **2022**, *12*, 3316. [Crossref]
57. Ilyas, M.; Muhammad, S.; Iqbal, J.; Amin, S.; Al-Sehemi, A. G.; Algarni, H.; Alarfaji, S. S.; Alshahrani, M. Y.; Ayub, K.; *Chem. Pap.* **2022**, *76*, 6271. [Crossref]
58. Arthur, D. E.; Elegbe, B. O.; Aroh, A. O.; Soliman, M.; *Bull. Natl. Res. Cent.* **2022**, *46*, 210. [Crossref]
59. Benhander, G. M.; Abdusalam, A. A. A.; *Chem. Africa* **2022**, *5*, 57. [Crossref]
60. Fu, L.; Ye, F.; Feng, Y.; Yu, F.; Wang, Q.; Wu, Y.; Zhao, C.; Sun, H.; Huang, B.; Niu, P.; Song, H.; Shi, Y.; Li, X.; Tan, W.; Qi, J.; Gao, G. F.; *Nat. Commun.* **2020**, *11*, 4417. [Crossref]
61. Lipinski, C. A.; *Drug Discovery Today: Technol.* **2004**, *1*, 337. [Crossref]
62. Tyagi, M.; Begnini, F.; Poongavanam, V.; Doak, B. C.; Kihlberg, J.; *Chem.-A Eur. J.* **2020**, *26*, 49. [Crossref]
63. Ungell, A.-L.; *Drug Dev. Ind. Pharm.* **1997**, *23*, 879. [Crossref]
64. Juliano, R. L.; Ling, V.; *Biochim. Biophys. Acta, Biomembr.* **1976**, *455*, 152. [Crossref]
65. Atanasov, A. G.; Zotchev, S. B.; Dirsch, V. M.; Supuran, C. T.; *Nat. Rev. Drug Discovery* **2021**, *20*, 200. [Crossref]
66. Bozhüyük, K. A. J.; Fleischhacker, F.; Linck, A.; Wesche, F.; Tietze, A.; Niesert, C.-P.; Bode, H. B.; *Nat. Chem.* **2018**, *10*, 275. [Crossref]
67. Rossi, S. E.; Erasmus, J. J.; McAdams, H. P.; Sporn, T. A.; Goodman, P. C.; *RadioGraphics* **2000**, *20*, 1245. [Crossref]
68. Abookleesh, F. L.; Al-Anzi, B. S.; Ullah, A.; *Molecules* **2022**, *27*, 903. [Crossref]
69. Españo, E.; Kim, J.; Lee, K.; Kim, J.-K.; *J. Microbiol.* **2021**, *59*, 959. [Crossref]
70. Rogosnitzky, M.; Okediji, P.; Koman, I.; *Pharmacol. Rep.* **2020**, *72*, 1509. [Crossref]
71. Tian, X.; Zhao, Q.; Chen, X.; Peng, Z.; Tan, X.; Wang, Q.; Chen, L.; Yang, Y.; *Front. Pharmacol.* **2022**, *13*, 817715. [Crossref]
72. Shen, J.-X.; Du, W.-W.; Xia, Y.-L.; Zhang, Z.-B.; Yu, Z.-F.; Fu, Y.-X.; Liu, S.-Q.; *Int. J. Mol. Sci.* **2023**, *24*, 4237. [Crossref]
73. Valipour, M.; Di Giacomo, S.; Di Sotto, A.; Irannejad, H.; *Int. J. Mol. Sci.* **2023**, *24*, 8789. [Crossref]
74. Alabbas, A. B.; Alamri, M. A.; *Saudi J. Biol. Sci.* **2022**, *29*, 526. [Crossref]
75. Stasiulewicz, A.; Maksymiuk, A. W.; Nguyen, M. L.; Bełza, B.; Sulkowska, J. I.; *Int. J. Mol. Sci.* **2021**, *22*, 3957. [Crossref]
76. Cheohen, C. F. A. R.; Esteves, M. E. A.; da Fonseca, T. S.; Leal, C. M.; Assis, F. L. F.; Campos, M. F.; Rebelo, R. S.; Allonso, D.; Leitão, G. G.; da Silva, M. L.; Leitão, S. G.; *Comput. Struct. Biotechnol. J.* **2023**, *21*, 1461. [Crossref]

Submitted: May 31, 2023
Published online: November 1, 2023